A model of electromagnetic electron phase-space holes and its application

J. B. Tao,[1] R. E. Ergun,[1] L. Andersson,[1] J. W. Bonnell,[2] A. Roux,[3] O. LeContel,[3] V. Angelopoulos,[4] J. P. McFadden,[2] D. E. Larson,[2] C. M. Cully,[5] H.-U. Auster,[6] K.-H. Glassmeier,[6] W. Baumjohann,[7] D. L. Newman,[8] and M. V. Goldman[8]

Received 25 August 2010; revised 11 August 2011; accepted 21 August 2011; published 15 November 2011.

[1] Electron phase-space holes (EHs) are indicators of nonlinear activities in space plasmas. Most often they are observed as electrostatic signals, but recently Andersson et al. [2009] reported electromagnetic EHs observed by the THEMIS mission in the Earth's plasma sheet. As a follow-up to Andersson et al. [2009], this paper presents a model of electromagnetic EHs where the $\delta\mathbf{E} \times \mathbf{B_0}$ drift of electrons creates a net current. The model is examined with test-particle simulations and compared to the electromagnetic EHs reported by Andersson et al. [2009]. As an application of the model, we introduce a more accurate method than the simplified Lorentz transformation of Andersson et al. [2009] to derive EH velocity (v_{EH}). The sizes and potentials of EHs are derived from v_{EH}, so an accurate derivation of v_{EH} is important in analyzing EHs. In general, our results are qualitatively consistent with those of Andersson et al. [2009] but generally with smaller velocities and sizes.

Citation: Tao, J. B., et al. (2011), A model of electromagnetic electron phase-space holes and its application, *J. Geophys. Res.*, *116*, A11213, doi:10.1029/2010JA016054.

1. Introduction

[2] In their original work, *Bernstein et al.* [1957] solved the exact one-dimensional, stationary Vlasov-Poisson system and demonstrated that an arbitrary traveling wave solution could be constructed with an appropriate distribution function of particles trapped in the potential-energy troughs. Even for the small-amplitude limit, they revealed that the trapped-particle distribution function does not possess an expansion in integral powers of the amplitude of the electrostatic potential as in conventional linearized theory, but rather one in half-integral powers. This special nonlinear nature of the trapped-particle distribution function was emphasized by the authors. Because of their fundamental work, a wave mode due to the nonlinear balance between the electrostatic potential and trapped particles is now often called a BGK mode. Along their derivation, they developed a framework to construct an exact solution to the stationary Vlasov-Poisson system by prescribing an arbitrary potential structure and then solving for the trapped-particle distribution function accordingly. This framework is now called the BGK method.

[3] Electron phase-space holes (EHs) first were discovered in early numerical simulations of electron two-stream instabilities and interpreted as a BGK mode [*Roberts and Berk*, 1967; *Morse and Nielson*, 1969]. Specifically, an EH is considered a purely nonlinear kinetic structure resulting from the self-consistent balance between a positive unipolar potential structure and an electron distribution that includes trapped particles.

[4] Since being discovered, EHs have been studied extensively. When presenting a statistical study of properties of small-amplitude electron phase-space holes observed by the POLAR mission in the high-altitude magnetosphere, *Franz et al.* [2005] provided a detailed historical review of the studies on EH, including numerical simulations [e.g., *Omura et al.*, 1996; *Newman et al.*, 2001; *Oppenheim et al.*, 2001], laboratory experiments [*Lynov et al.*, 1979; *Saeki et al.*, 1979], theoretical investigations [e.g., *Dupree*, 1982; *Collantes and Turikov*, 1988], and space observations [e.g., *Matsumoto et al.*, 1994; *Ergun et al.*, 1998a; *Cattell et al.*, 1999, and references therein]. More observations and experiments of EHs were reported recently [*Cattell et al.*, 2005; *Retinò et al.*, 2006; *Deng et al.*, 2006; *Pickett et al.*, 2009; *Khotyaintsev et al.*, 2010; *Hashimoto et al.*, 2010; *Fox et al.*, 2008; *Lefebvre et al.*, 2010].

[5] Numerical simulations have shown that the generation mechanisms of EHs generally fall into two categories:

[1]Laboratory for Atmospheric and Space Physics, University of Colorado at Boulder, Boulder, Colorado, USA.
[2]Space Sciences Laboratory, University of California, Berkeley, California, USA.
[3]Laboratoire de Physique des Plasmas, CNRS/Ecole Polytechnique/UPMC/Paris-Sud 11, Saint-Maur-des-Fossés, France.
[4]IGPP/ESS, University of California, Los Angeles, California, USA.
[5]Swedish Institute of Space Physics, Uppsala, Sweden.
[6]Institut für Geophysik und Extraterrestrische Physik, Technische Universität Braunschweig, Braunschweig, Germany.
[7]Space Research Institute, Austrian Academy of Sciences, Graz, Austria.
[8]Center for Integrated Plasma Studies, University of Colorado at Boulder, Boulder, Colorado, USA.

0148-0227/11/2010JA016054

electron-electron beam instabilities, with two [e.g., *Omura et al.*, 1996; *Singh et al.*, 2000] or more components [e.g., *Lu et al.*, 2005], and current-driven (Buneman) instabilities [e.g., *Singh and Schunk*, 1982; *Drake et al.*, 2003; *Goldman et al.*, 2008; *Che et al.*, 2009, 2010]. In the latter case, EHs could result directly from the nonlinear evolution of the Buneman instability [e.g., *Drake et al.*, 2003] or from a secondary process, namely, double layers, driven by the Buneman instability [e.g., *Singh and Schunk*, 1984; *Singh et al.*, 1987; *Newman et al.*, 2001, 2008]. In any case, a pre-existing electron beam, either from initial conditions [e.g., *Miyake et al.*, 1998; *Umeda et al.*, 2006] or accelerated by other processes in the simulations like double layers [e.g., *Singh*, 2000; *Newman et al.*, 2001] or magnetic reconnection [*Drake et al.*, 2003], is presented as a free-energy source for the instabilities. In space plasmas, electron beams most often are from nonlinear, energetic processes, making EHs an excellent indicator of such processes.

[6] EHs most often are observed as localized electrostatic signals with no observable magnetic field signal. However, some auroral observations [*Mozer et al.*, 1997; *Ergun et al.*, 1998a, 1998b] showed EHs with both electric field and magnetic field signals. In these papers, the magnetic field signal associated with EHs were assumed to be in the perpendicular direction. (The terms "parallel" and "perpendicular" are with respect to the ambient magnetic field throughout this paper except as otherwise noted.) *Ergun et al.* [1998a, 1998b] interpreted the magnetic field signal as the Lorentz transformation of the perpendicular electric fields of a rapidly moving electrostatic EH. Recently, *Andersson et al.* [2009] reported THEMIS [*Angelopoulos*, 2008] observations of electromagnetic EHs in the plasma sheet. One uniqueness of their observations is that those electromagnetic EHs have magnetic field signals in both the perpendicular and parallel components. As in work by *Ergun et al.* [1998b, 1998a], *Andersson et al.* [2009] concluded that the perpendicular magnetic field signal primarily resulted from the Lorentz transformation of the perpendicular electric fields of the EHs. As for the parallel magnetic field signals, they interpreted them as results from the $\delta\mathbf{E} \times \mathbf{B_0}$ drift of electrons passing through the EHs, where $\delta\mathbf{E}$ is the electric field of EHs, and $\mathbf{B_0}$ is the ambient magnetic field. (Electromagnetic fields are reference-frame dependent. In this paper, we generally use primed symbols, such as $\delta\mathbf{E}'$ and $\delta\mathbf{B}'$, to indicate electromagnetic fields in the EH frame, and non-primed symbols, such as $\delta\mathbf{E}$ and $\delta\mathbf{B}$, to indicate those in the spacecraft frame. Strictly speaking, the $\delta\mathbf{E}$ in $\delta\mathbf{E} \times \mathbf{B_0}$ drift should be $\delta\mathbf{E}'$. However, we use the expression $\delta\mathbf{E} \times \mathbf{B_0}$ for the ease of notation throughout this paper.)

[7] The $\delta\mathbf{E} \times \mathbf{B_0}$ drift associated with EHs in magnetized plasmas have been discussed in a few theoretical papers [*Terry et al.*, 1990; *Jovanovic and Horton*, 1993; *Chen and Parks*, 2002]. Both *Terry et al.* [1990] and *Jovanovic and Horton* [1993] considered EHs with sizes larger than the ion gyroradius and velocities between the ion and electron thermal velocities using the drift kinetic approximation in which ions are subject to the electromagnetic fields of EHs. *Chen and Parks* [2002] considered 3-D EHs with sizes much larger than the electron gyroradius and velocities much larger than the ion thermal velocity in magnetized plasmas. They argued that the ion dynamics could be ignored in that circumstance and that the $\delta\mathbf{E} \times \mathbf{B_0}$ drift of electrons would not affect the BGK equilibria in EHs assuming an azimuthal symmetry for the EHs. In these papers, the magnetic field signals were not specifically studied, possibly because there had not been observations or simulations to motivate theoretical work. In a later paper, *Umeda et al.* [2004] demonstrated magnetic field signals of EHs resulting from $\delta\mathbf{E} \times \mathbf{B_0}$ drift of electrons in 2-D electromagnetic PIC simulations. In work by *Umeda et al.* [2004], the perpendicular magnetic field signals primarily resulted from the $\delta\mathbf{E} \times \mathbf{B_0}$ drift of electrons as they did not take into account the Lorentz-transformation effect. Generally, although 3-D EHs in magnetized plasmas have been investigated to some extent, a comprehensive 3-D perspective of electromagnetic EHs as reported by *Andersson et al.* [2009] is still missing. In this paper, we present a 3-D model of electromagnetic EHs to fill this gap.

[8] In our model, a perturbation magnetic field is induced by a current from the $\delta\mathbf{E} \times \mathbf{B_0}$ drift of electrons passing through the EH. One key question is whether such a current could be established. The $\mathbf{E} \times \mathbf{B}$ drift does not necessarily result in net current if both ions and electrons are subject to this drift. However, we show that, at certain time scale, only electrons but not ions can establish the $\delta\mathbf{E} \times \mathbf{B_0}$ drift current.

[9] Assuming the perpendicular magnetic field components from $\delta\mathbf{E} \times \mathbf{B_0}$ drift of electrons could be ignored, *Andersson et al.* [2009] derived the velocities relative to the spacecraft of EHs (v_{EH}) with a simplified Lorentz transformation:

$$\delta B_y \approx +\frac{v_{EH}}{c^2}\delta E_x \tag{1}$$

$$\delta B_x \approx -\frac{v_{EH}}{c^2}\delta E_y \tag{2}$$

where δB_x, δB_y, δE_x and δE_y are perpendicular field components of EHs in Field Aligned Coordinates (FAC), c is the speed of light, and v_{EH} is assumed to be in the z direction (along $\mathbf{B_0}$). Although this derivation gives a rough estimate of the EH velocity, it has not been examined in detail. One difficulty is that the observations show that the $\delta E_x(\delta E_y)$ signal and the $\delta B_y(\delta B_x)$ signal do not always peak simultaneously as they should according to equations (1) and (2). However, this misalignment can be explained if the contribution from the $\delta\mathbf{E} \times \mathbf{B_0}$ drift of electrons to δB_x and δB_y is not negligible. As such, we develop a more accurate method to derive v_{EH} that takes into account the perpendicular magnetic field components from $\delta\mathbf{E} \times \mathbf{B_0}$ drift of electrons. The mean v_{EH} from this new method is ~20% smaller compared to that of *Andersson et al.* [2009], although this new method produces qualitatively consistent results with those previously reported.

[10] The organization of the rest of this paper is as follows. In Section 2, we provide a brief review of the observations of the electromagnetic EHs reported by *Andersson et al.* [2009]. In Section 3, we present a detailed description of our model including the underlying assumptions of the model. In Section 4, we investigate the formation of the $\delta\mathbf{E} \times \mathbf{B_0}$ drift current of charged particles passing through an EH with test-particle simulations. In Section 5, we introduce a more accurate method for deriving v_{EH}. We then re-derive the velocities, potentials, and parallel sizes with this new method,

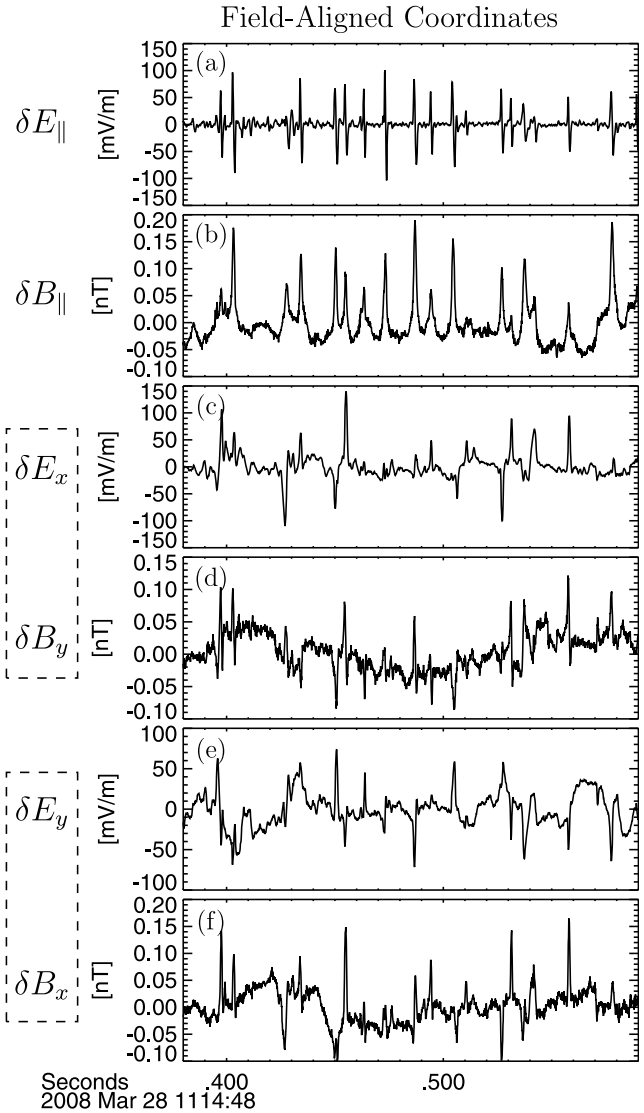

Figure 1. ~0.2 s of high temporal resolution data of electromagnetic perturbation $\delta\mathbf{E}$ and $\delta\mathbf{B}$ (filtered from ~5 Hz to ~3.3 kHz; sample rate 8192 s^{-1}) from a ~16 s wave burst. The data are plotted in Field-Aligned Coordinates (FAC). (a and b) The subscript $\parallel$ indicates that the corresponding component is of the same direction of $\mathbf{B_0}$. x and y components are perpendicular to $\mathbf{B_0}$. The two dashline boxes group (c) δE_x and (d) δB_y, (e) δE_y and (f) δB_x together respectively because the two components of each group are related by the simplified Lorentz transformation (equations (1) and (2)). (Similar to Figure 2 of *Andersson et al.* [2009].)

and show some EH examples in Section 6. This paper is finalized with a section of discussion and a summary.

2. Review of Observations

[11] *Andersson et al.* [2009] reported electromagnetic EHs that were observed by the THEMIS probe A in the plasma sheet at ($x_{GSM} \sim -6.0\ R_E$, $y_{GSM} \sim 7.4\ R_E$, $z_{GSM} \sim -1.6\ R_E$) on March 28th, 2008. These electromagnetic EHs are within a ~16 s "wave burst" from 11:14:41 UT to 11:47:57 UT. The term "wave burst" refers to THEMIS field data with high temporal resolution (sampled at ~8 kHz or ~16 kHz) on short durations ($\lesssim$ 20 s). There were no time delays observed in the individual voltage signals from the electric field instrument, so the EHs had speed greater than 1000 km/s. During the event, the magnitude of the ambient magnetic field (B_0) is ~50 nT, the plasma number density (n_0) is ~0.02 cm^{-3}, the ion temperature (T_i) is ~3 keV, the parallel electron temperature ($T_{e\parallel}$) is ~8 keV, and the perpendicular electron temperature ($T_{e\perp}$) is ~5 keV. The particle measurements are based on the on-board THEMIS electrostatic analyzer (ESA) which measures electrons and ions with energy less than ~30 keV [*McFadden et al.*, 2008a]. For this particular event, there is noticeable ion differential energy flux reaching the upper energy limit of the ESA instrument, indicating that the ion temperature may be underestimated [*McFadden et al.*, 2008b]. The uncertainties of the particle measurements are within 25%.

[12] Figure 1 shows ~0.2 s of the electromagnetic perturbations $\delta\mathbf{E}$ and $\delta\mathbf{B}$ (filtered from ~5 Hz to ~3.3 kHz; sampled at 8192 Hz) from the ~16s wave burst. The data are in Field-Aligned Coordinates (FAC) which are based on the DC magnetic field data from the THEMIS Fluxgate Magnetometer [*Auster et al.*, 2008]. The $\delta\mathbf{E}$ signals are from the THEMIS Electric Field Instrument [*Bonnell et al.*, 2008], while the $\delta\mathbf{B}$ signals are from the THEMIS Search Coil Magnetometer [*Roux et al.*, 2008]. The x and y components are perpendicular to $\mathbf{B_0}$. The solitary spiky bipolar $\delta E_{\parallel}$ signals shown in Figure 1a are defining signatures of EHs [e.g., *Matsumoto et al.*, 1994; *Ergun et al.*, 1998a] used to search for EHs in observations. One can see that the polarities of $\delta E_{\parallel}$ of these EHs are identical, indicating that they are traveling in the same direction and are likely from the same source. These electromagnetic EHs have positive, unipolar $\delta B_{\parallel}$ signals with amplitudes up to ~0.2 nT, as shown in Figure 1b. Figures 1c–1f show that the δE_x and δB_y signals are correlated while the δE_y and δB_y signals are anti-correlated for these electromagnetic EHs. The amplitudes of all three $\delta\mathbf{E}$ components of EHs are unusually large (up to ~100 mV/m) compared to most THEMIS observations and Cluster observations [*Cattell et al.*, 2005; *Pickett et al.*, 2004] in the Earth's plasma sheet.

[13] By fitting the EH signals with a Gaussian profile and using the corresponding Gaussian amplitude, *Andersson et al.* [2009] applied the simplified Lorentz transformation to obtain that $v_{EH} \sim 10^8$ m/s, $L_{\parallel} \sim 100$ km, mean $\Delta\Phi \sim 3$ kV and maximum $\Delta\Phi \sim 10$ kV, where $\Delta\Phi$ is the amplitude of EH potentials along the spacecraft track. In addition, they argued that the shape of those EHs was likely to be elongated based on the fact that some of the electromagnetic EHs have ΔE_x or ΔE_y greater than $\Delta E_{\parallel}$, where ΔE_x and ΔE_y are the peak amplitudes of δE_x and δE_y signals of EHs respectively, and $\Delta E_{\parallel}$ is the half peak-to-peak difference of $\delta E_{\parallel}$ signal of EHs. (In this paper, we generally use the lower-case delta (δ) to indicate a full field signal as a function of time or space, and the upper-case delta (Δ) to indicate the peak amplitude except as otherwise noted.)

3. Model Description and Formulation

[14] In this section, we describe a 3-D model of electromagnetic EHs and formulate it based on a cylindrically

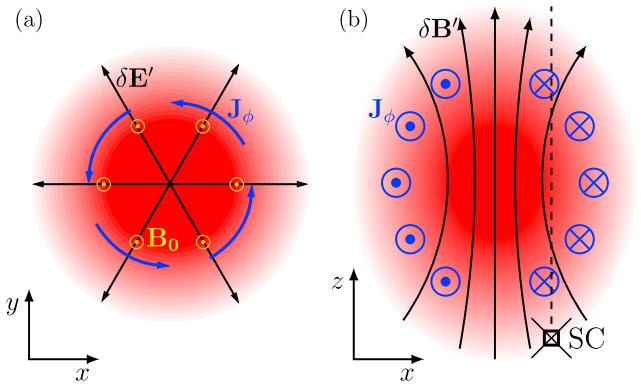

Figure 2. A qualitative illustration of our EH model in the EH frame showing the cross-sections in the FAC (a) x-y plane and (b) x-z plane respectively where the red areas represent the EH. In Figure 2a, the black arrows represent the electrostatic fields $\delta\mathbf{E}'$ from the electrostatic potential of the EH, and the yellow dot-circles represent the ambient magnetic fields $\mathbf{B_0}$ pointing out of the paper. The blue arrows and symbols in Figures 2a and 2b respectively represent the azimuthal current $\mathbf{J}_\phi$ generated by the $\delta\mathbf{E} \times \mathbf{B_0}$ drift of electrons. In Figure 2b the black curved arrows crossing the EH represent the magnetic field $\delta\mathbf{B}'$ induced by $\mathbf{J}_\phi$. The dashline in Figure 2b represents an imaginary spacecraft track, and the small object below it represents the spacecraft (SC).

symmetric Gaussian potential profile (same as *Chen et al.* [2004])

$$\Phi = \Phi_0 e^{-\frac{r^2}{2l_\perp^2}} e^{-\frac{z^2}{2l_\parallel^2}}, \tag{3}$$

where Φ_0 is the central potential of the EH, r and z are cylindrical coordinates corresponding to the FAC ($r = \sqrt{x^2+y^2}$), and $l_\perp(l_\parallel)$ is the half perpendicular(parallel) size of the EH ($L_\perp = 2l_\perp$, $L_\parallel = 2l_\parallel$).

[15] Two assumptions are made for the model.

[16] 1. Only electrons but not ions can establish a $\delta\mathbf{E} \times \mathbf{B_0}$ drift current when passing through an EH. This is valid for $t_{ce} \lesssim \delta t \ll t_{ci}$ and $\rho_e \ll L_\perp \ll \rho_i$ where δt is the transit time of an EH bypassing the spacecraft, $t_{ce}(t_{ci})$ the electron (ion) gyroperiod, and $\rho_e(\rho_i)$ the electron(ion) gyroradius. The justification of this assumption for the electromagnetic EHs reported by *Andersson et al.* [2009] is addressed in Section 4.

[17] 2. The electron density is assumed to be uniform. This is valid for $\frac{e\Delta\Phi}{T} \ll \frac{L_{EH}^2}{\lambda_D^2}$ according to the Poisson's equation, where L_{EH} is the scale size of the EHs, and T and λ_D are the temperature and Debye length of the background plasmas. As shown later, this condition is satisfied for the electromagnetic EHs reported by *Andersson et al.* [2009]. We note that this assumption is specifically for simplifying the analytic formulation of the model. Relaxing this assumption will not change the qualitative nature of our model but make the formulation more complex.

[18] Figure 2 illustrates the model in the EH frame. Figures 2a and 2b are two cross-sections of the EH model in the FAC x-y plane and x-z plane respectively. The red areas represent the EH. In Figure 2a, the black arrows represent the electrostatic fields ($\delta\mathbf{E}'$) from the electrostatic potential of the EH, and the yellow dot-circles represent the ambient magnetic fields ($\mathbf{B_0}$) pointing out of the paper. $\delta\mathbf{E}'$ fields point radially outwards because the electrostatic potential peaks positively at the center of the EH. The blue arrows and symbols in Figures 2a and 2b, respectively, represent the azimuthal current $\mathbf{J}_\phi$ generated by the $\delta\mathbf{E} \times \mathbf{B_0}$ drift of electrons. The black curved arrows crossing the EH in Figure 2b represent the magnetic field $\delta\mathbf{B}'$ induced by $\mathbf{J}_\phi$. The dashed line in Figure 2b represents an imaginary spacecraft track, and the small object below it represents the spacecraft (SC). One can see that the parallel component of $\delta\mathbf{B}'$ in our model is predominantly of the same direction of $\mathbf{B_0}$, and hence the spacecraft should mostly record positive unipolar $\delta B_\parallel$ structures as shown in Figure 1.

[19] Given equation (3), one obtains $\delta\mathbf{E}'$ and $\mathbf{J}_\phi$ as

$$\delta\mathbf{E}' = -\nabla\Phi = \frac{r}{l_\perp^2}\Phi\hat{\mathbf{r}} + \frac{z}{l_\parallel^2}\Phi\hat{\mathbf{z}}, \tag{4}$$

$$\mathbf{J}_\phi \approx -en_0\frac{\delta\mathbf{E}' \times \mathbf{B}_0}{B_0^2} = \frac{en_0 r}{B_0 l_\perp^2}\Phi\hat{\phi}, \tag{5}$$

where $\hat{\mathbf{r}}$, $\hat{\mathbf{z}}$, and $\hat{\phi}$ are the unit vectors of the cylindrical coordinate system. $\delta\mathbf{B}'$ is obtained with the Biot-Savart law [*Jackson*, 1998a]

$$\begin{aligned}\delta\mathbf{B}'(\mathbf{x}) &= \frac{\mu_0}{4\pi}\int \mathbf{J}_\phi(\mathbf{x}') \times \frac{\mathbf{x}-\mathbf{x}'}{|\mathbf{x}-\mathbf{x}'|^3} d^3x' \\ &= \frac{en_0\mu_0}{B_0 4\pi}\int \frac{x'}{l_\perp^2}\Phi\hat{\phi} \times \frac{\mathbf{x}-\mathbf{x}'}{|\mathbf{x}-\mathbf{x}'|^3} d^3x'\end{aligned} \tag{6}$$

In general, numerical integration is required to obtain $\delta\mathbf{B}'$ from equation (6) for an arbitrary location inside the EH. However, the central $\delta\mathbf{B}'$ can be obtained analytically as

$$\delta\mathbf{B}'(r=0, z=0) = \frac{e\Phi_0\mu_0 n_0}{B_0} g(l_\perp/l_\parallel)\hat{\mathbf{z}} \tag{7}$$

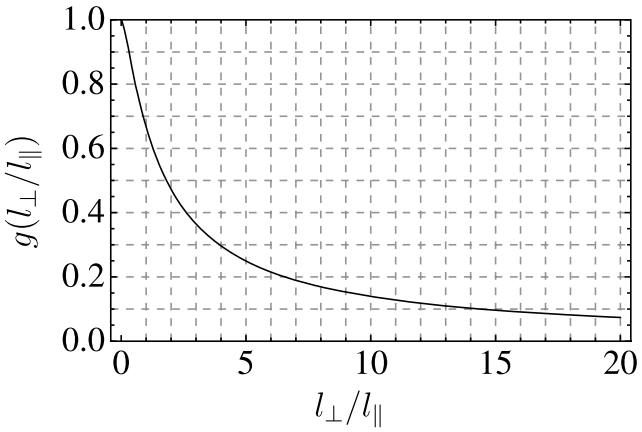

Figure 3. The geometric factor g as a function of $l_\perp/l_\parallel$.

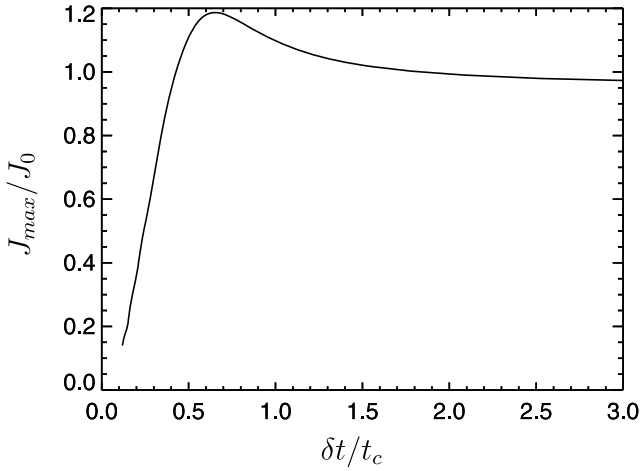

Figure 4. The effect of the transit time to the formation of the $\delta\mathbf{E} \times \mathbf{B_0}$ drift current from test-particle simulations. $J_{\max}$ is obtained in the perpendicular plane at the center of the EH. J_0 is the theoretical maximum of J_ϕ according to equation (5). δt is the transit time through the EH, and t_c is the gyroperiod of particles.

where

$$g(l_\perp/l_\parallel) = \mathrm{Re}\left[\frac{1-\frac{l_\perp^2}{l_\parallel^2}+\frac{l_\perp^2}{l_\parallel^2}\arccos\left(\frac{l_\parallel}{l_\perp}\right)\sqrt{\frac{l_\perp^2}{l_\parallel^2}-1}}{\left(1-\frac{l_\perp^2}{l_\parallel^2}\right)^2}\right] \quad (8)$$

Note that the dimensionless factor g only depends on the ratio $l_\perp/l_\parallel$ which characterizes the shape of the EH and hence is called a geometric factor. Figure 3 shows the behavior of g as a function of $l_\perp/l_\parallel$.

4. Formation of $\delta\mathbf{E} \times \mathbf{B_0}$ Drift Current

[20] A key assumption to the model is that only electrons but not ions could establish a $\delta\mathbf{E} \times \mathbf{B_0}$ drift current when passing through an EH. Since the $\delta\mathbf{E} \times \mathbf{B_0}$ drift current stems from the gyromotion of charged particles, establishing the ion current requires that the perpendicular size of the EH is large enough to contain enough gyroorbits and that the transit time of ions through the EH is a significant fraction of the gyroperiod. The transit time through an EH is approximately equal to the duration of the EH in the satellite data. For the electromagnetic EHs in the ~16s wave burst, the transit time is ~1 ms, and the ion gyroperiod is ~1 s, so it is reasonable to neglect the ion current in this case. On the other hand, the corresponding electron gyroperiod (~1 ms) is very close to the transit time. It is not clear if the electrons could establish a $\delta\mathbf{E} \times \mathbf{B_0}$ drift current in this timescale. To address this issue, we investigate the formation of the $\delta\mathbf{E} \times \mathbf{B_0}$ drift current of charged particles passing through an EH with test-particle simulations. As discussed by *Chen and Parks* [2002], the $\delta\mathbf{E} \times \mathbf{B_0}$ drift of electrons does not substantially affect the BGK equilibrium of an 3-D EH in magnetized plasmas. Therefore, a test-particle simulation model is appropriate for this investigation.

4.1. Simulation Model

[21] The test-particle code we have developed is a 2-D, particle-in-cell (PIC) code, in which we use the widely used Boris method to update particle velocities and a first-order shape function to obtain the current density on the grid [see *Birdsall and Langdon*, 1985]. Particles are initialized with uniform density in the x-y plane plane outside the EH and moving toward it with Maxwellian velocity distributions in v_x and v_y but with a uniform $v_\parallel$ (equivalent to v_z). To cover a full distribution of $v_\parallel$, multiple runs are required.

[22] With periodic boundary conditions, the simulation plane expands over a $N_x \times N_y = 100 \times 100$ grid with $-L/2 \le x \le L/2$ and $-L/2 \le y \le L/2$, where L is large enough to completely cover the EH. The number of total particles is 20 million with ~2000 per cell.

4.2. Simulation Results

[23] The major diagnostics of the investigation is the maximum current density in the simulation plane ($J_{\max}$) normalized by the theoretical maximum current density (J_0) according to equation (5). $J_{\max}$ is calculated as the average of the current density over the ring between $r = l_\perp - 0.1l_\perp$ and $r = l_\perp + 0.1l_\perp$, a region where the maximum $\delta\mathbf{E} \times \mathbf{B_0}$ drift current is expected.

[24] As mentioned earlier, multiple runs are required to cover the full distribution of $v_\parallel$. The $J_{\max}$ of a full distribution of $v_\parallel$ is calculated as

$$J_{\max} = \int_{\infty}^{-\infty} J_{\max} f_\parallel(v_\parallel; v_{EH})\, dv_\parallel, \quad (9)$$

where $f_\parallel(v_\parallel; v_{EH}) = \frac{1}{\sqrt{2\pi v_t^2}} \exp[-\frac{(v_\parallel + v_{EH})^2}{2v_t^2}]$, v_t is the thermal velocity of the particles, and $J_{\max}$ is obtained from a single simulation run.

[25] Figure 4 shows the effect of the transit time (δt) with respect to the gyroperiod of the particles (t_c) to the formation of the $\delta\mathbf{E} \times \mathbf{B_0}$ drift current. δt is calculated by $L_\parallel/v_{EH}$ where $L_\parallel$ is 20 gyroradii of the particles. One can see that the $\delta\mathbf{E} \times \mathbf{B_0}$ drift current quickly drops as δt decreases when $\delta t/t_c$ is less than ~0.5. When $\delta t/t_c \gtrsim 1$, the simulation results approximately match the theoretical results. The overshoot between $\delta t/t_c = 0.5$ and $\delta t/t_c = 1$ is a phase effect indicating that the ensemble of particle gyromotions enhances the $\delta\mathbf{E} \times \mathbf{B_0}$ drift current in this time range. For the EHs in ~16s wave burst, the transit times through the EHs are approximately equal to the electron gyroperiod. According to Figure 4, we conclude that the electron $\delta\mathbf{E} \times \mathbf{B_0}$ drift current could be established in those EHs.

5. A More Accurate Method for Deriving v_{EH}

[26] In this section, we examine the use of the Lorentz transformation to derive v_{EH} of the electromagnetic EHs in the ~16s wave burst and introduce a more accurate method to derive v_{EH}.

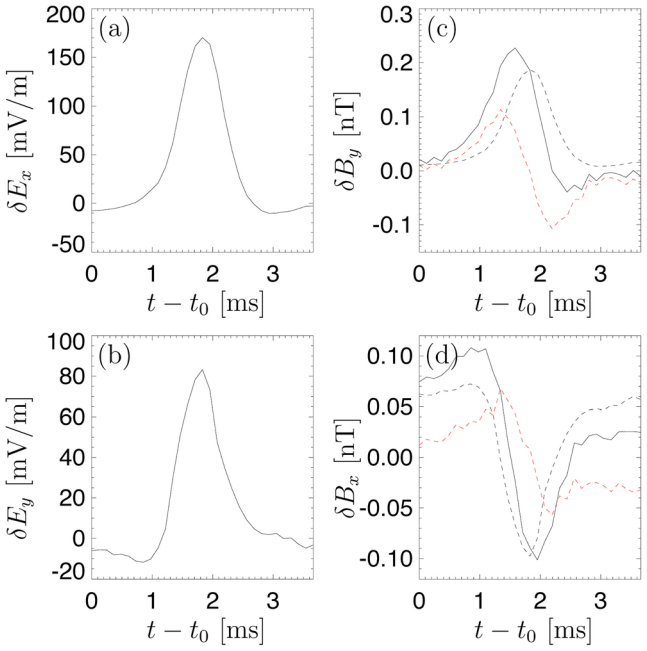

Figure 5. An example of the linear fit introduced in Section 5, where t_0 is 2008-03-28/11:14:48.0616 in the x-axis labels. (a) The observed δE_x. (b) The observed δE_y. (c) The observed δB_y (solid line), δB_y^{fit} (black, dashed line), δB_y^{res} (red, dashed line). (d) The observed δB_x (solid line), δB_x^{fit} (black, dashed line), δB_x^{res} (red, dashed line).

[27] The exact Lorentz transformation from the EH frame to the spacecraft frame in FAC is the following (*Jackson* [1998b], changed to SI)

$$\begin{aligned} \delta E_\parallel &= \delta E'_\parallel & \delta B_\parallel &= \delta B'_\parallel \\ \delta E_x &= \gamma\left(\delta E'_x + v_{EH}\delta B'_y\right) & \delta B_x &= \gamma\left(\delta B'_x - \frac{v_{EH}}{c^2}\delta E'_y\right) \\ \delta E_y &= \gamma\left(\delta E'_y - v_{EH}\delta B'_x\right) & \delta B_y &= \gamma\left(\delta B'_y + \frac{v_{EH}}{c^2}\delta E'_x\right) \end{aligned} \quad (10)$$

where $\gamma = (1 - v_{EH}^2/c^2)^{-1/2}$. Substituting the expressions of δE_x and δE_y into the expressions of δB_y and δB_x respectively and taking a weak relativity approximation (i.e., $\gamma \approx 1$), one obtains

$$\delta B_x \approx \delta B'_x - v_{EH}\frac{\delta E_y}{c^2} \quad (11)$$

$$\delta B_y \approx \delta B'_y + v_{EH}\frac{\delta E_x}{c^2} \quad (12)$$

(As shown later, the EHs in this paper are only weakly relativistic.)

[28] As shown in Figure 2, the perpendicular components of $\delta\mathbf{B}'$, $\delta B'_x$ and $\delta B'_y$, are typically bipolar along spacecraft trajectories. As a superposition of $\delta B'_y$ (bipolar) and $v_{EH}\delta E'_x/c^2$ (unipolar), δB_y can be an asymmetric bipolar signal with one dominant peak, depending on the relative location of the spacecraft trajectory inside the EH. A simple Gaussian-fit amplitude of such a structure to determine ΔB_y can overestimate $v_{EH}\delta E'_x/c^2$ and results in an overestimated v_{EH} with the simplified Lorentz transformation. So is the case for δB_x. To resolve this issue, we introduce a more accurate method to derive v_{EH}. In this method, the measured δB_y signals are fitted with the following linear model

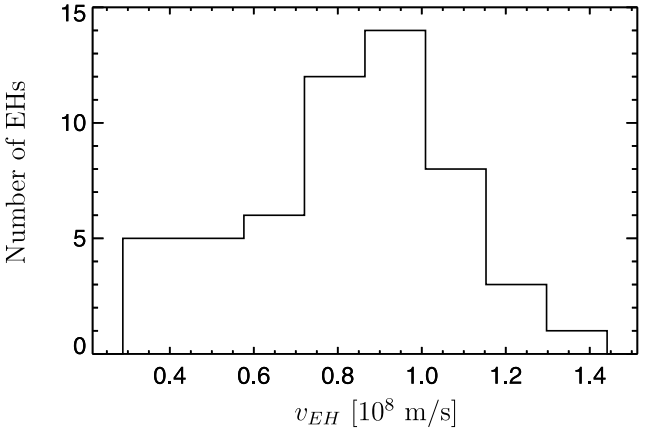

Figure 6. Histogram of v_{EH}.

$$\delta B_y^{fit} = v\frac{\delta E_x}{c^2}, \quad (13)$$

$$\delta B_x^{fit} = -v\frac{\delta E_y}{c^2}. \quad (14)$$

where v is an estimate of v_{EH}, while the residue δB_y^{res} (= $\delta B_y - \delta B_y^{fit}$) and δB_x^{res}(= $\delta B_x - \delta B_x^{fit}$) are an estimate of $\delta B'_y$ and $\delta B'_x$ respectively. The two fits of v_{EH} are combined by choosing the one with a smaller uncertainty.

[29] Figure 5 shows an example of the linear fit. As an estimate of $\delta B'_y$ and $\delta B'_x$ respectively, the bipolar feature of δB_y^{res} and δB_x^{res} is consistent with our model. In addition, one can see that the peak of $\delta B_y(\delta B_x)$ differs from that of $\delta E_x(\delta E_y)$ as previously discussed.

6. Statistical Results of EH Velocities, Potentials, Parallel Sizes, and EH Examples

[30] This section presents statistical results of the velocities, potentials, and sizes of the electromagnetic EHs in the ~16s wave burst using the method introduced in Section 5.

[31] The first step of this work is to select EHs in the ~16s wave burst. The following criteria are applied in this step.

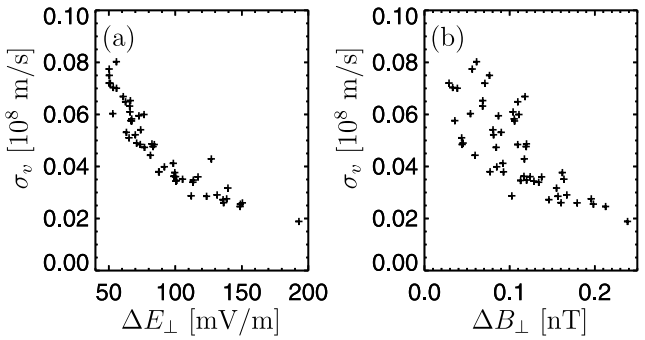

Figure 7. (a) σ_v versus $\Delta E_\perp$. (b) σ_v versus $\Delta B_\perp$.

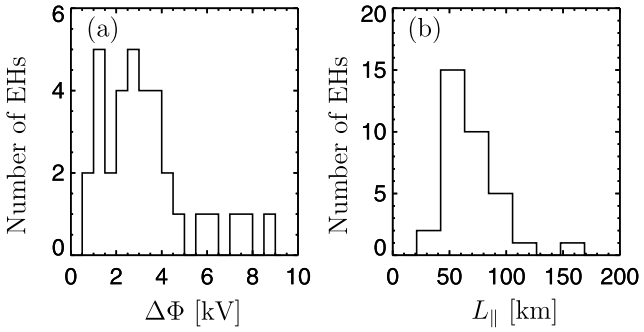

Figure 8. Histograms of (a) EH potential $\Delta\Phi$ and (b) parallel size $L_{\|}$.

[32] 1. The magnitude of each peak of the bipolar $\delta E_{\|}$ must be greater than 10 mV/m and three times the local standard deviation that is calculated over a 201-data-point window (25 ms).

[33] 2. The peak-to-peak interval of the bipolar $\delta E_{\|}$ must be less than 2 ms and greater than the local electron gyroperiod (≈0.71 ms).

[34] 3. The polarity of the bipolar $\delta E_{\|}$ must be positive-then-negative in time as shown in Figure 1a.

[35] 4. $\Delta E_{\perp}$ must be greater than 50 mV/m, where $\Delta E_{\perp}$ is either $\Delta E_x(\equiv \max[\delta E_x] - \min[\delta E_x])$ or $\Delta E_y(\equiv \max[\delta E_y] - \min[\delta E_y])$, depending on which one produces a better fit.

[36] These selection criteria result in 54 EH samples from the ~16s wave burst. Each EH sample consists of 31 data points (4 ms). In the above criteria, the first one makes use of the solitary feature of EHs. The second one is to make sure that only one EH is selected at a time as the peak-to-peak interval of EHs (δt) is generally less than 1 ms in this event, and that electrons can have sufficient time to establish $\delta\mathbf{E} \times \mathbf{B_0}$ drift current as shown in Figure 4. The third one ensures that the selected EHs travel in the same direction and hence are likely from the same source. The fourth one restricts the results with relatively small uncertainties because increasing $\Delta E_{\perp}$ can improve the goodness of the linear fit model as shown by equations (11) and (12).

6.1. Velocity, Potential, and Parallel Size

[37] Figure 6 shows the distribution of the derived v_{EH}. The mean v_{EH} is 0.83×10^8 m/s, roughly 20% less than that of *Andersson et al.* [2009], which supports the argument that the Gaussian-fit method could result in an overestimation when the perpendicular components of $\delta\mathbf{B}'$ is not generally negligible. From Figure 6 one can verify that $\gamma \approx 1$ is valid for the EHs in the ~16s wave burst.

[38] Figure 7 shows the relations of σ_v, uncertainty of v_{EH}, with $\Delta E_{\perp}$ and $\Delta B_{\perp}$ respectively, where $\Delta B_{\perp}$ is either $\Delta B_x(\equiv \max[\delta B_x] - \min[\delta B_x])$ or $\Delta B_y(\equiv \max[\delta B_y] - \min[\delta B_y])$, depending on which one is selected to derive v_{EH}. One can see that the trend of σ_v decreasing as $\Delta E_{\perp}$ increases is relatively tighter than that as $\Delta B_{\perp}$ increases. This trend difference is consistent with equations (11) and (12) because increasing $\Delta E_{\perp}$ immediately improves the goodness of the linear fit model but increasing $\Delta B_{\perp}$ does not necessarily have that effect due to the existence of $\delta B'_x$ and $\delta B'_y$.

[39] Once the velocity is derived, the potential and size of an EH can be derived by fitting the $\delta E_{\|}$ with the derivative of a Gaussian [e.g., see *Ergun et al.*, 1998b]. Figure 8 shows the potentials and sizes of the 54 EHs. Because the fourth selection criterion mentioned above confines the perpendicular offset of the spacecraft trajectory through an EH roughly in a region of large $\delta E_{\perp}$, one can see that $\Delta\Phi$ is relatively centered around 3 kV. But $\Delta\Phi$ can reach up to ~9 kV occasionally, suggesting that the central potentials of the EHs are mostly similar but can be very strong in a few EHs. The mean of $\Delta\Phi$ is ~3.2 kV. Moreover, one can see that the distribution of $L_{\|}$ is more concentrated than that of $\Delta\Phi$, which confirms that the potential of the EHs can be roughly described with a cylindrically symmetric Gaussian because in that situation $L_{\|}$ is roughly independent on the perpendicular offset to the center of an EH but $\Delta\Phi$ is sensitive to that offset. The mean of $L_{\|}$ is ~68 km. Additionally, the perpendicular sizes of the EHs are generally comparable to parallel sizes because the measurements of $\Delta E_{\perp}$ are generally comparable to those of $\Delta E_{\|}$.

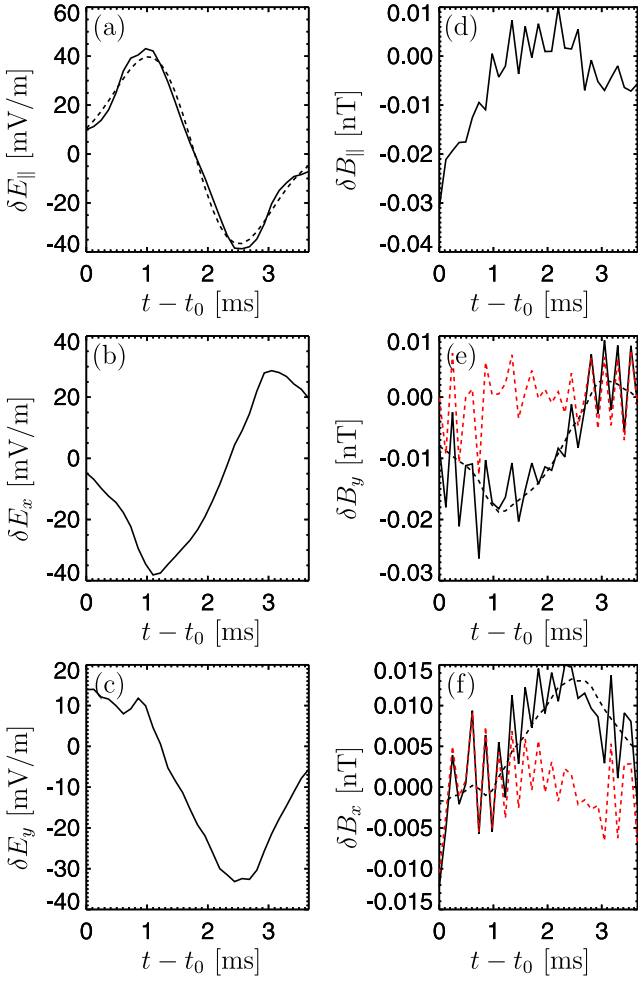

Figure 9. (a–f) An example of a slow EH, where t_0 is 2008-03-28/11:14:54.1617 in the x-axis labels. The dashed line in Figure 9a is a fit of $\delta_{\|}$ with the derivative of a Gaussian. The formats of Figures 9e and 9f are the same as those in Figures 5c and 5d, respectively. The velocity is 2.90×10^7 m/s from the fit of δB_y, and 2.85×10^7 m/s from the fit δB_x, with the first one chosen to be the final value because its uncertainty is smaller.

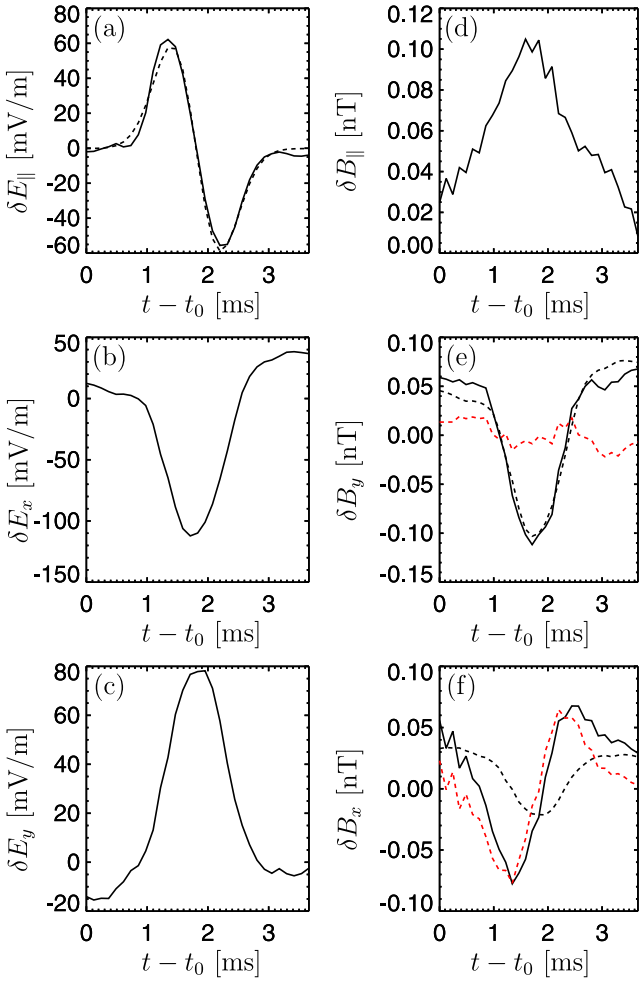

Figure 10. An example of a fast EH, where t_0 is 2008-03-28/11:14:48.2664 in the x-axis labels. The format is the same as Figure 9. The velocity is 1.07×10^8 m/s from the fit of δB_y, and 0.53×10^8 m/s from the fit δB_x, with the first one chosen to be the final value because its uncertainty is smaller.

6.2. EH Examples

[40] Figure 9 shows a relatively slow EH with a velocity of 2.90×10^7 m/s. The estimated potential and $L_\parallel$ are ~1.4 kV and ~43 km respectively. With $n_0 = 0.02$ cm^{-3}, $B_0 = 50$ nT, and $g = 0.5$, our model in Section 3 gives $\Delta B_\parallel \lesssim 0.055$ nT according to equation (7). The amplitude of δB_z is difficult to estimate in this case because of its irregular shape. However, if one takes the range of the δB_z ($\max[\delta B_z] - \min[\delta B_z]$) 0.04 nT as an estimate of the amplitude of δB_z, the observation and the model is roughly in agreement. In the figure, one can see that the δE_x and δE_y signals do not peak at the center of the EH as they would in an ideal cylindrically symmetric case. One possible reason is that the transformation of the signals into FAC is not perfect, due to the uncertainty in determining $\mathbf{B_0}$, so that there are contributions left in δE_x and δE_y from the parallel component. Another possibility is that the shape of this EH is irregular so that the sizes of EH in x and y dimensions are different. EHs with irregular shapes are not uncommon in simulations [*Lu et al.*, 2008]. Note that these two possibilities are not exclusive. Both possibilities could contribute to the results shown in Figure 9.

[41] Figure 10 shows a relatively fast EH with a velocity of 1.07×10^8 m/s. The estimated potential and $L_\parallel$ are ~4.2 kV and ~87 km respectively. The observed amplitude of δB_z is ~0.09 nT as shown in Figure 10d. With the same background parameters and assuming the perpendicular offset of the spacecraft trajectory is roughly $l_\perp$, our model gives an estimate of $\Delta B_z \sim 0.1$ nT, consistent with the observation. One interesting fact in the figure is that δB_y is well fitted by δE_x but δB_x is not by δE_y. This suggests that $\delta B_x'$ is relatively more important than $\delta B_y'$, which further suggests that the size of EH in y dimension is larger than in x dimension. (This can be understood from Figure 2b. Imagine an extreme case that the y-dimension size of the EH is infinite, in which $\delta B_y'$ would be zero.) Additionally, the irregularity of the internal structure of the EH can contribute to the results. However, it is difficult to infer such an irregularity based on a single spacecraft crossing.

[42] In addition to the 54 EH samples, we fortunately found a relatively clean center-crossing (small $\Delta E_\perp$ and large $\Delta E_\parallel$) EH example as shown in Figure 11. The esti-

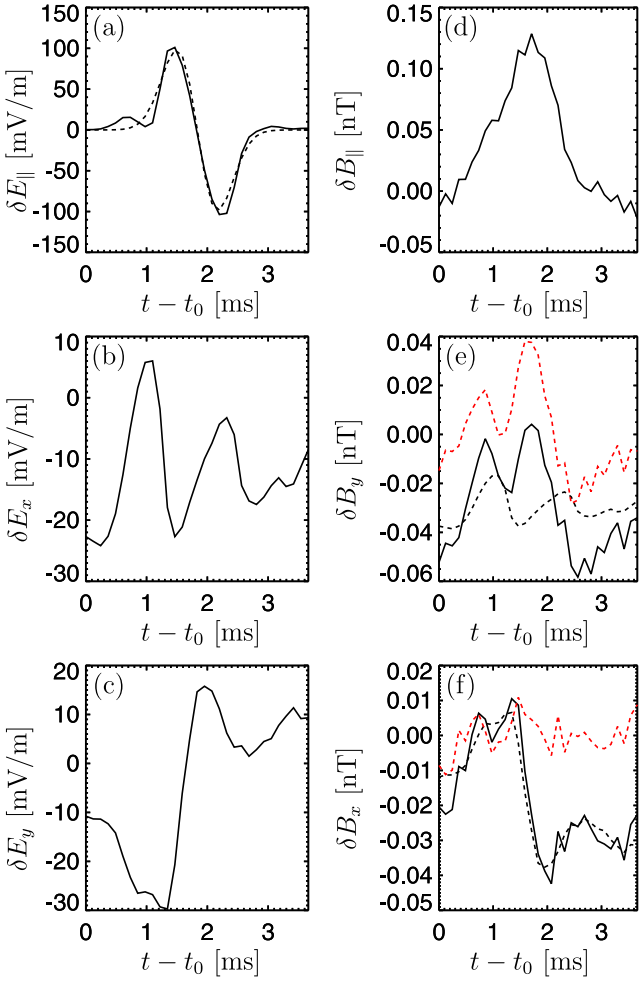

Figure 11. An example of central EH crossing, where t_0 is 2008-03-28/11:14:48.4716 in the x-axis labels. The format is the same as Figure 9. The final estimated velocity is 8.7×10^7 m/s from δB_x and δE_y.

mated potential is ~4.8 kV, which is higher than the average value shown in Section 6.1 as expected, and the size ~59 km. The observed amplitude of δB_z is roughly 0.15 nT, and our model gives an estimate 0.19 nT without a perpendicular offset correction. Considering the uncertainties in the perpendicular offset and the EH shape, the model and the observation are in a fairly good agreement.

7. Discussion

[43] The use of our model is limited to the following conditions. First, no ion $\delta\mathbf{E} \times \mathbf{B_0}$ drift current is established. Second, the transit time through the EH is comparable to or greater than the local electron gyroperiod and the perpendicular size of the EH must be much greater than the local electron gyroradius. (Given the background electron gyroradius $\rho_e \approx 3.4$ km, one can verify that the perpendicular sizes of the EHs in the ~16s wave burst were much larger than the local electron gyroradius.) In observations, the relation between the transit time and the electron/ion gyroperiods usually can be determined directly. Unfortunately, the size of EHs is generally not easy to estimate. For relatively slowly moving EHs, one can use the time delay method [*Franz et al.*, 1998] to determine v_{EH} and eventually estimate $L_\perp$. Modern instruments can determine v_{EH} over 1000 km/s with this method. For fast-moving EHs, if there are noticeable unipolar $\delta B_\parallel$ signals associated with EHs, it is likely that the electron $\delta\mathbf{E} \times \mathbf{B_0}$ drift currents are established in the EHs.

[44] One assumption we made in Section 3 is that the density is uniform. As mentioned earlier, this is valid for $\frac{e\Delta\Phi}{T} \ll \frac{L_{EH}^2}{\lambda_D^2}$. Because the size of the EHs are derived independently on this assumption, one can use the results from Section 6.1 to verify the assumption. With $T \sim 5$ keV, $\Delta\Phi \sim 3.2$ kV, $L_{EH} \sim 70$ km, $\lambda_D \sim 4$ km, one gets $e\Delta\Phi/T \sim 0.64$ and $L_{EH}^2/\lambda_D^2 \sim 300$. Therefore, the condition for the uniform density assumption is well satisfied.

[45] *Du et al.* [2011] recently reported 2-D electromagnetic simulations of EHs. In their simulations, $\mathbf{B_0}$ was along x axis and the computation was carried on the x-y plane. They found unipolar δB_x and bipolar δB_y perturbations from the $\delta\mathbf{E} \times \mathbf{B_0}$ drift of electrons, which strongly supports our model.

8. Summary

[46] In this paper, we introduced a model of electromagnetic EHs where the $\delta\mathbf{E} \times \mathbf{B_0}$ drift of electrons creates a net current. Then we examined the formation of the $\delta\mathbf{E} \times \mathbf{B_0}$ drift current in an EH and demonstrated that a net current from electron $\delta\mathbf{E} \times \mathbf{B_0}$ drift could be established in the electromagnetic EHs reported by *Andersson et al.* [2009]. Then, we introduced a more accurate method to derive v_{EH}. We re-derived v_{EH} with this method for the ~16s wave burst and concluded that the v_{EH} of *Andersson et al.* [2009] was overestimated by ~20%. The potentials and sizes of those EHs were re-derived accordingly. We propose the use of the more accurate method for future studies.

[47] **Acknowledgments.** This work was supported by NASA grants for THEMIS and FAST, by the German DLR, by French institutes CNES and CNRS-INSU, and by a NASA Earth and Space Sciences Fellowship (10-Helio10F-0004). The authors wish to thank the entire THEMIS team.

[48] Masaki Fujimoto thanks Nagendra Singh and another reviewer for their assistance in evaluating this paper.

References

Andersson, L., et al. (2009), New features of electron phase space holes observed by the THEMIS mission, *Phys. Rev. Lett.*, *102*, 225004, doi:10.1103/PhysRevLett.102.225004.

Angelopoulos, V. (2008), The THEMIS mission, *Space Sci. Rev.*, *141*, 5–34, doi:10.1007/s11214-008-9336-1.

Auster, H. U., et al. (2008), The THEMIS fluxgate magnetometer, *Space Sci. Rev.*, *141*, 235–264, doi:10.1007/s11214-008-9365-9.

Bernstein, I. B., J. M. Greene, and M. D. Kruskal (1957), Exact nonlinear plasma oscillations, *Phys. Rev.*, *108*, 546–550, doi:10.1103/PhysRev.108.546.

Birdsall, C. K., and A. B. Langdon (1985), *Plasma Physics Via Computer Simulation*, McGraw-Hill, New York.

Bonnell, J. W., F. S. Mozer, G. T. Delory, A. J. Hull, R. E. Ergun, C. M. Cully, V. Angelopoulos, and P. R. Harvey (2008), The Electric Field Instrument (EFI) for THEMIS, *Space Sci. Rev.*, *141*, 303–341, doi:10.1007/s11214-008-9469-2.

Cattell, C. A., et al. (1999), Comparisons of Polar satellite observations of solitary wave velocities in the plasma sheet boundary and the high altitude cusp to those in the auroral zone, *Geophys. Res. Lett.*, *26*, 425–428, doi:10.1029/1998GL900304.

Cattell, C., et al. (2005), Cluster observations of electron holes in association with magnetotail reconnection and comparison to simulations, *J. Geophys. Res.*, *110*, A01211, doi:10.1029/2004JA010519.

Che, H., J. F. Drake, M. Swisdak, and P. H. Yoon (2009), Nonlinear development of streaming instabilities in strongly magnetized plasma, *Phys. Rev. Lett.*, *102*, 145004, doi:10.1103/PhysRevLett.102.145004.

Che, H., J. F. Drake, M. Swisdak, and P. H. Yoon (2010), Electron holes and heating in the reconnection dissipation region, *Geophys. Res. Lett.*, *37*, L11105, doi:10.1029/2010GL043608.

Chen, L., and G. K. Parks (2002), BGK electron solitary waves in 3D magnetized plasma, *Geophys. Res. Lett.*, *29*(9), 1331, doi:10.1029/2001GL013385.

Chen, L., D. J. Thouless, and J. Tang (2004), Bernstein Greene Kruskal solitary waves in three-dimensional magnetized plasma, *Phys. Rev. E*, *69*(5), 055401, doi:10.1103/PhysRevE.69.055401.

Collantes, J. R., and V. A. Turikov (1988), Stability of solitary BGK waves, *Phys. Scr.*, *38*, 825–828, doi:10.1088/0031-8949/38/6/013.

Deng, X. H., et al. (2006), Observations of electrostatic solitary waves associated with reconnection by Geotail and Cluster, *Adv. Space Res.*, *37*, 1373–1381, doi:10.1016/j.asr.2005.05.129.

Drake, J. F., M. Swisdak, C. Cattell, M. A. Shay, B. N. Rogers, and A. Zeiler (2003), Formation of electron holes and particle energization during magnetic reconnection, *Science*, *299*, 873–877, doi:10.1126/science.1080333.

Du, A., M. Wu, Q. Lu, C. Huang, and S. Wang (2011), Transverse instability and magnetic structures associated with electron phase space holes, *Phys. Plasmas*, *18*(3), 032104, doi:10.1063/1.3561796.

Dupree, T. H. (1982), Theory of phase-space density holes, *Phys. Fluids*, *25*, 277–289, doi:10.1063/1.863734.

Ergun, R. E., et al. (1998a), FAST satellite observations of large-amplitude solitary structures, *Geophys. Res. Lett.*, *25*, 2041–2044, doi:10.1029/98GL00636.

Ergun, R. E., C. W. Carlson, J. P. McFadden, F. S. Mozer, L. Muschietti, I. Roth, and R. J. Strangeway (1998b), Debye-scale plasma structures associated with magnetic-field-aligned electric fields, *Phys. Rev. Lett.*, *81*, 826–829, doi:10.1103/PhysRevLett.81.826.

Fox, W., M. Porkolab, J. Egedal, N. Katz, and A. Le (2008), Laboratory observation of electron phase-space holes during magnetic reconnection, *Phys. Rev. Lett.*, *101*, 255003, doi:10.1103/PhysRevLett.101.255003.

Franz, J. R., P. M. Kintner, and J. S. Pickett (1998), Polar observations of coherent electric field structures, *Geophys. Res. Lett.*, *25*, 1277–1280, doi:10.1029/98GL50870.

Franz, J. R., P. M. Kintner, J. S. Pickett, and L.-J. Chen (2005), Properties of small-amplitude electron phase-space holes observed by Polar, *J. Geophys. Res.*, *110*, A09212, doi:10.1029/2005JA011095.

Goldman, M. V., D. L. Newman, and P. Pritchett (2008), Vlasov simulations of electron holes driven by particle distributions from PIC reconnection simulations with a guide field, *Geophys. Res. Lett.*, *35*, L22109, doi:10.1029/2008GL035608.

Hashimoto, K., et al. (2010), Electrostatic solitary waves associated with magnetic anomalies and wake boundary of the Moon observed by KAGUYA, *Geophys. Res. Lett.*, *37*, L19204, doi:10.1029/2010GL044529.

Jackson, J. D. (1998a), *Classical Electrodynamics*, 3rd ed., chap. 5, p. 178, John Wiley, New York.

Jackson, J. D. (1998b), *Classical Electrodynamics*, 3rd ed., chap. 11, p. 558, John Wiley, New York.

Jovanovic, D., and W. Horton (1993), Quasi-three-dimensional electron holes in magnetized plasmas, *Phys. Fluids B*, *5*, 433–439, doi:10.1063/1.860528.

Khotyaintsev, Y. V., A. Vaivads, M. André, M. Fujimoto, A. Retinò, and C. J. Owen (2010), Observations of slow electron holes at a magnetic reconnection site, *Phys. Rev. Lett.*, *105*, 165002, doi:10.1103/PhysRevLett.105.165002.

Lefebvre, B., L. Chen, W. Gekelman, P. Kintner, J. Pickett, P. Pribyl, S. Vincena, F. Chiang, and J. Judy (2010), Laboratory measurements of electrostatic solitary structures generated by beam injection, *Phys. Rev. Lett.*, *105*, 115001, doi:10.1103/PhysRevLett.105.115001.

Lu, Q. M., D. Y. Wang, and S. Wang (2005), Generation mechanism of electrostatic solitary structures in the Earth's auroral region, *J. Geophys. Res.*, *110*, A03223, doi:10.1029/2004JA010739.

Lu, Q. M., B. Lembege, J. B. Tao, and S. Wang (2008), Perpendicular electric field in two-dimensional electron phase-holes: A parameter study, *J. Geophys. Res.*, *113*, A11219, doi:10.1029/2008JA013693.

Lynov, J. P., P. Michelsen, H. L. Pecseli, J. Juul Rasmussen, K. Saeki, and V. A. Turikov (1979), Observations of solitary structures in a magnetized, plasma loaded waveguide, *Phys. Scr.*, *20*, 328–335, doi:10.1088/0031-8949/20/3-4/005.

Matsumoto, H., H. Kojima, T. Miyatake, Y. Omura, M. Okada, I. Nagano, and M. Tsutsui (1994), Electrotastic solitary waves (ESW) in the magnetotail: BEN wave forms observed by Geotail, *Geophys. Res. Lett.*, *21*, 2915–2918, doi:10.1029/94GL01284.

McFadden, J. P., C. W. Carlson, D. Larson, M. Ludlam, R. Abiad, B. Elliott, P. Turin, M. Marckwordt, and V. Angelopoulos (2008a), The THEMIS ESA plasma instrument and in-flight calibration, *Space Sci. Rev.*, *141*, 277–302, doi:10.1007/s11214-008-9440-2.

McFadden, J. P., C. W. Carlson, D. Larson, J. Bonnell, F. Mozer, V. Angelopoulos, K. Glassmeier, and U. Auster (2008b), THEMIS ESA first science results and performance issues, *Space Sci. Rev.*, *141*, 477–508, doi:10.1007/s11214-008-9433-1.

Miyake, T., Y. Omura, H. Matsumoto, and H. Kojima (1998), Two-dimensional computer simulations of electrostatic solitary waves observed by Geotail spacecraft, *J. Geophys. Res.*, *103*, 11,841–11,850, doi:10.1029/98JA00760.

Morse, R. L., and C. W. Nielson (1969), One-, two-, and three-dimensional numerical simulation of two-beam plasmas, *Phys. Rev. Lett.*, *23*, 1087–1090, doi:10.1103/PhysRevLett.23.1087.

Mozer, F. S., R. Ergun, M. Temerin, C. Cattell, J. Dombeck, and J. Wygant (1997), New features of time domain electric-field structures in the auroral acceleration region, *Phys. Rev. Lett.*, *79*, 1281–1284, doi:10.1103/PhysRevLett.79.1281.

Newman, D. L., M. V. Goldman, R. E. Ergun, and A. Mangeney (2001), Formation of double layers and electron holes in a current-driven space plasma, *Phys. Rev. Lett.*, *87*, 255001, doi:10.1103/PhysRevLett.87.255001.

Newman, D. L., L. Andersson, M. V. Goldman, R. E. Ergun, and N. Sen (2008), Influence of suprathermal background electrons on strong auroral double layers: Vlasov-simulation parameter study, *Phys. Plasmas*, *15*(7), 072902, doi:10.1063/1.2938753.

Omura, Y., H. Matsumoto, T. Miyake, and H. Kojima (1996), Electron beam instabilities as generation mechanism of electrostatic solitary waves in the magnetotail, *J. Geophys. Res.*, *101*, 2685–2697, doi:10.1029/95JA03145.

Oppenheim, M. M., G. Vetoulis, D. L. Newman, and M. V. Goldman (2001), Evolution of electron phase-space holes in 3D, *Geophys. Res. Lett.*, *28*, 1891–1894, doi:10.1029/2000GL012383.

Pickett, J., L. Chen, S. Kahler, O. Santolík, D. Gurnett, B. Tsurutani, and A. Balogh (2004), Isolated electrostatic structures observed throughout the Cluster orbit: Relationship to magnetic field strength, *Ann. Geophys.*, *22*, 2515–2523, doi:10.5194/angeo-22-2515-2004.

Pickett, J. S., et al. (2009), Electrostatic solitary waves in current layers: From Cluster observations during a super-substorm to beam experiments at the LAPD, *Nonlinear Processes Geophys.*, *16*, 431–442.

Retinò, A., et al. (2006), Structure of the separatrix region close to a magnetic reconnection X-line: Cluster observations, *Geophys. Res. Lett.*, *33*, L06101, doi:10.1029/2005GL024650.

Roberts, K. V., and H. L. Berk (1967), Nonlinear evolution of a two-stream instability, *Phys. Rev. Lett.*, *19*, 297–300, doi:10.1103/PhysRevLett.19.297.

Roux, A., O. Le Contel, C. Coillot, A. Bouabdellah, B. de La Porte, D. Alison, S. Ruocco, and M. C. Vassal (2008), The search coil magnetometer for THEMIS, *Space Sci. Rev.*, *141*, 265–275, doi:10.1007/s11214-008-9455-8.

Saeki, K., P. Michelsen, H. L. Pécseli, and J. J. Rasmussen (1979), Formation and coalescence of electron solitary holes, *Phys. Rev. Lett.*, *42*, 501–504, doi:10.1103/PhysRevLett.42.501.

Singh, N. (2000), Electron holes as a common feature of double-layer-driven plasma waves, *Geophys. Res. Lett.*, *27*, 927–930, doi:10.1029/1999GL003709.

Singh, N., and R. W. Schunk (1982), Current-driven double layers and the auroral plasma, *Geophys. Res. Lett.*, *9*, 1345–1348, doi:10.1029/GL009i012p01345.

Singh, N., and R. W. Schunk (1984), Plasma response to the injection of an electron beam, *Plasma Phys. Controlled Fusion*, *26*, 859–890, doi:10.1088/0741-3335/26/7/003.

Singh, N., H. Thiemann, and R. W. Schunk (1987), Simulations of auroral plasma processes—Electric fields, waves and particles, *Planet. Space Sci.*, *35*, 353–395, doi:10.1016/0032-0633(87)90162-0.

Singh, N., S. M. Loo, B. E. Wells, and C. Deverapalli (2000), Three-dimensional structure of electron holes driven by an electron beam, *Geophys. Res. Lett.*, *27*, 2469–2472, doi:10.1029/2000GL003766.

Terry, P. W., P. H. Diamond, and T. S. Hahm (1990), The structure and dynamics of electrostatic and magnetostatic drift holes, *Phys. Fluids B*, *2*, 2048–2063, doi:10.1063/1.859426.

Umeda, T., Y. Omura, and H. Matsumoto (2004), Two-dimensional particle simulation of electromagnetic field signature associated with electrostatic solitary waves, *J. Geophys. Res.*, *109*, A02207, doi:10.1029/2003JA010000.

Umeda, T., Y. Omura, T. Miyake, H. Matsumoto, and M. Ashour-Abdalla (2006), Nonlinear evolution of the electron two-stream instability: Two-dimensional particle simulations, *J. Geophys. Res.*, *111*, A10206, doi:10.1029/2006JA011762.

L. Andersson, R. E. Ergun, and J. B. Tao, Laboratory for Atmospheric and Space Physics, University of Colorado at Boulder, 1234 Innovation Dr., Boulder, CO 80303-7814, USA. (jianbao.tao@colorado.edu)

V. Angelopoulos, IGPP/ESS, University of California, Box 951567, 2712 Geology Bldg., Los Angeles, CA 90095-1567, USA.

H.-U. Auster and K.-H. Glassmeier, Institut für Geophysik und Extraterrestrische Physik, Technische Universität Braunschweig, Mendelssohnstr. 3, D-38106 Braunschweig, Germany.

W. Baumjohann, Space Research Institute, Austrian Academy of Sciences, Schmiedlstr. 6, A-8042 Graz, Austria.

J. W. Bonnell, D. E. Larson, and J. P. McFadden, Space Sciences Laboratory, University of California, 7 Gauss Way, Berkeley, CA 94720-7450, USA.

C. M. Cully, Swedish Institute of Space Physics, Box 537, SE-75121 Uppsala, Sweden.

M. V. Goldman and D. L. Newman, Center for Integrated Plasma Studies, University of Colorado at Boulder, UCB 390, Boulder, CO 80309-0390, USA.

O. LeContel and A. Roux, Laboratoire de Physique des Plasmas, CNRS/Ecole Polytechnique/UPMC/Paris-Sud 11, 4 avenue de Neptune, F-94107 Saint-Maur-des-Fossés, France.